RESEARCH ARTICLE

Improving heat transfer and water recovery performance in high-moisture flue gas condensation using silicon carbide membranes

Chao Ji[1] | Li Li[2] | Hong Qi[1]

[1]State Key Laboratory of Materials-Oriented Chemical Engineering, Membrane Science and Technology Research Center, Nanjing Tech University, Nanjing, China

[2]Hongyi Ceramic Membranes Research Institute, Nanjing Hongyi Ceramic Nanofiltration Membranes Co., Ltd, Nanjing, China

Correspondence
Hong Qi, State Key Laboratory of Materials-Oriented Chemical Engineering, Membrane Science and Technology Research Center, Nanjing Tech University, Nanjing 210009, Jiangsu, China.
Email: hqi@njtech.edu.cn

Summary

Desulfurated flue gas in coal-fired power plants contains profuse water vapor and latent heat, the recovery of which is crucial. Herein, a novel use of silicon carbide (SiC) membranes to construct a transport membrane condenser (TMC) for simultaneous water and waste heat recovery from high-moisture flue gas is reported. The performances of water and heat recovery were systematically compared between typical dense heat exchange materials (304 stainless steel and perfluoroalkoxy [PFA]) and porous ceramic membranes (Al_2O_3 membrane and SiC membrane). Porous ceramic membranes showed higher heat transfer performance than dense materials, suggesting a non-negligible mass transfer effect on heat transfer. Compared with the Al_2O_3 membrane, the SiC membrane exhibited better water and heat recovery performance because of its superior thermal conductivity. Using the SiC membrane as the heat exchange material, a water flux of 11.3-44.4 kg·m^{-2}·h^{-1} and a water recovery efficiency of 46.5%-76.9% were achieved. The thermal resistance from the gas boundary layer dominated the heat transfer process in SiC membrane condensers as the thermal resistances from the membrane and condensate film were markedly reduced. This study forms a basis for future investigations on heat transfer enhancement of membrane condensers used for industrial moisture recovery.

KEYWORDS

flue gas dehumidifcation, heat transfer, silicon carbide membrane, transport membrane condenser, water recovery

1 | INTRODUCTION

Considerable flue gas is produced during industrial processes such as chemical production, power generation, drying, flush quenching, and wet scrubbing. Typically, the flue gas, containing moisture and thermal energy, is directly exhausted into the atmosphere.[1] Until 2040, about 40% of the world's electricity will come from coal annually.[2] For coal-fired power plants, 3%-8% of the fuel calorific value is lost in the form of the thermal energy of the flue gas.[3] Water vapor constitutes 12%-16% of the flue gas.[4] Hydrocarbon fuel combustion and wet flue gas desulfurization process (WFGD) are the main sources of moisture. The annual amount of water vapor discharged after WFGD exceeds 100 million tons in China.[5] If 20% of

Abbreviations: GTI, Gas Technology Institute; TMC, transport membrane condenser; WFGD, wet flue gas desulfurization; PVDF, poly (vinylidene fluoride); SPEEK, sulfonated poly(ether ether ketone); PFA, perfluoroalkoxy; LMTD, logarithmic mean temperature difference.

the water vapor and waste heat can be recovered, power plants would be self-sufficient with processed water.[6] Meanwhile, the utilization ratio of thermal energy would obviously be improved. In addition, the direct emission of high-humidity flue gas leads to visual pollution and a series of environmental problems around power plants, such as colored smoke plumes, gypsum rain,[7] and low atmospheric visibility.[8] Capturing water vapor from flue gas is key to solving these issues. From energy and environment prospects, clean coal technology[9] and waste-to-energy[10] have receiving a growing attention. Therefore, it is imperative to recycle moisture from high-humidity flue gas exhausted by coal-fired power plants.

Methods for recycling moisture from high-humidity flue gas include condensation, absorption, and membrane technology.[11] Condensation technology are widely used for moisture recovery from flue gas.[12-15] However, conventional metal heat exchangers have some limitations.[16] (a) Low-temperature corrosion will reduce the lifespan of heat exchangers and raise maintenance cost. (b) Further treatment is required for low-quality recovered water. (c) The mixture of condensate and fly ash may form a fouling layer on the tube wall of metal heat exchangers seriously affecting heat transfer efficiency. The fluorine plastic heat exchanger, which can resist acid contaminant corrosion and ash fouling, may be a substitute for the metal heat exchanger.[15] However, low heat conductivity restricts the efficiency of using fluorine plastic heat exchangers, and thus, modified plastic needs to be developed.[17] In addition, the feasibility of other methods for flue gas treatment is verified through experiments, such as open absorption system and hybrid heat pump system. Open absorption system could recover moisture and waste heat from gas-fired flue gases. However, sulfides and oxynitrides from coal-fired flue gas may deteriorate the recovery performance.[18] The greatest challenge is to reduce the energy consumption for absorbent regeneration. Boiler efficiency can be significantly improved using a novel hybrid heat pump system, which is composed of two air preheaters, a two-stage heat exchanging unit, and a mechanical compression heat pump. But the installation cost of the system is expensive.[19]

Currently, membrane condensation has been investigated as a promising technology for moisture recovery from flue gas.[20-22] Compared with conventional metal heat exchangers, membrane condensers exhibit the advantages of remarkable acid corrosion resistance, high quality of recovered water, and easy cleaning. Three types of membranes based on different transfer mechanisms have been investigated. (a) Dense organic membranes: the sulfonated poly(ether ether ketone) (SPEEK) membranes,[23] which are hydrophilic and have a high water vapor selectivity, are used to separate water vapor from other gases in the flue gas via the solution-diffusion mechanism. However, the poor mechanical strengths of these membranes and high energy consumption of the joint vacuum equipment should be considered for practical use. (b) Porous organic membranes: the condensate can be retained in the retentate side of hydrophobic poly(vinylidene fluoride) (PVDF) membranes,[24] whereas dehumidified gases permeate through the membranes. However, the air coolant and organic heat exchange materials may lead to limited condensing heat transfer performance. (c) Porous ceramic membranes: the Gas Technology Institute (GTI) in the United States introduced the novel concept of TMC based on hydrophilic nanoporous ceramic membranes for water capture, where the water vapor condenses in pores via capillary condensation.[25] The TMC unit was used to extract water vapor and waste heat from coal-fired flue gas during an 800-hours continuous test,[4] and a water recovery efficiency of 40%-55% was achieved. Subsequently, a series of comparable experiments demonstrated that the mass transfer coefficients of nanoporous membrane tubes are 60%-80% higher than those of impermeable stainless steel tubes at the same mean temperature difference.[26] Further research on the efficacy of TMCs was performed by Hu et al.[27] and Chen et al.[28] Owing to the excellent chemical stability, thermostability, mechanical strength, and heat transfer performance of porous ceramic membranes, TMCs have great potential for moisture recovery in the complex flue environment.[29]

Previously, we investigated the feasibility of using mono-[30] and 19-channel[31] tubular ceramic membranes for water recovery. Then, we compared the heat and mass transfer performances of ceramic membranes with selective layers coated on the inner or outer side of the substrate, respectively.[32] Finally, we used the outer-side coated mono-channel ceramic membranes to construct TMCs for the pilot study.[33] Based on the pilot study, 1 m^2 of the Al_2O_3 ceramic membrane can only handle 330 m$^3 \cdot$h^{-1} of flue gas because of the low temperature difference between the flue gas and cooling water.[13] For a typical 300 MW thermal power plant, the flue gas flowrate is about 10^6 m$^3 \cdot$h^{-1}.[34] An extensive membrane area is required for flue gas condensation, which results in large space occupation and high investment in membrane condensers. Thus, future investigations should focus on enhancing the heat transfer performance of TMCs to reduce the membrane area.

The thermal conductivity of heat exchange materials significantly affects the heat transfer performance of condensers.[35] Currently, mass-produced ceramic membranes are made of Al_2O_3, TiO_2, and ZrO_2;[36] among these, Al_2O_3 membranes are widely used to construct ceramic membrane-based condensers. However, the thermal conductivity of Al_2O_3 is relatively low. Table 1 summarizes

TABLE 1 Thermal conductivities of different materials

| Material (single crystal)	Thermal conductivity/ $W \cdot m^{-1} \cdot K^{-1}$
ZrO_2	2
TiO_2	10
Al_2O_3	30
AlN	320
Si_3N_4	320
SiC	490

the thermal conductivities of different materials at room temperature,[37-39] revealing that SiC, which has extremely high thermal conductivity, may be a potentially suitable material to construct TMCs for water recovery from flue gas. The thermal conductivity of ceramic materials is affected by many factors such as pores.[40] Preparing SiC membrane with high thermal conductivity for flue gas condensation is the focus of future work.

In this work, the SiC membrane was first proposed for water and waste heat recovery from the high-moisture flue gas following WFGD in coal-fired power plants. The heat and mass transfer performances of the SiC membrane were compared with those of the Al_2O_3 membrane, 304 stainless steel, and PFA. In addition, the effects of operational parameters, including air flowrate, flue gas temperature, cooling water flowrate, cooling water temperature, and transmembrane pressure difference, on water recovery performance were studied. Thermal resistances in the membrane condenser were also analyzed and calculated. Our findings may provide novel insights into heat transfer enhancement of TMCs used for water and waste heat recovery from flue gas.

2 | EXPERIMENT

2.1 | Materials

Four types of heat exchange materials, including a tubular SiC membrane, tubular Al_2O_3 membrane, 304 stainless steel tube, and PFA tube, were used in our experiment (Figure 1). The dense 304 stainless steel tube and PFA tube were obtained from local hardware shops. The porous tubular ceramic membranes were provided by Nanjing Hongyi Ceramic Nanofiltration Membranes Co., Ltd., China. The separation layer of the tubular ceramic membranes was coated on the inner side of the substrate. The average pore sizes of the SiC and Al_2O_3 membranes are both 0.4 μm. The geometric parameters of the experimental materials are listed in Table 2.
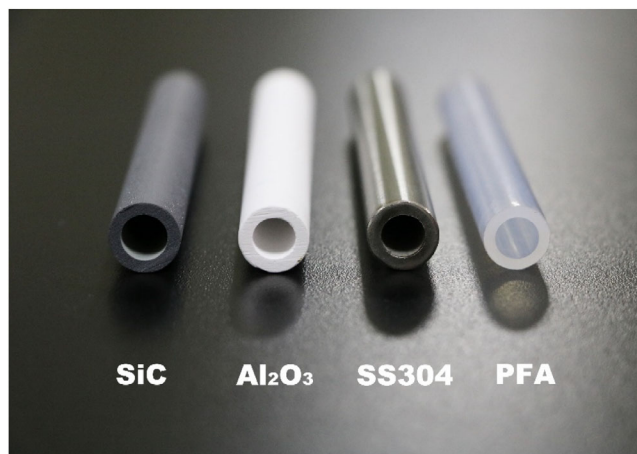
FIGURE 1 Photographs of the experimental materials [Colour figure can be viewed at wileyonlinelibrary.com]

TABLE 2 Parameters of the experimental materials

Material	Effective length (mm)	Inner diameter (mm)	Wall thickness (mm)
Tubular SiC membrane	90	8	2.4
Tubular Al_2O_3 membrane	90	8	2.4
304 stainless steel tube	90	8	2.4
PFA tube	90	8	2

2.2 | Experimental setup

Flue gas condensation experiments were conducted using a home-made bench-scale condensation system (Figure 2). The operational parameters applied in this work are listed in Table 3. The shell-and-tube condenser was horizontally arranged; this condenser comprised a heat exchange tube (i.e., SiC membrane, Al_2O_3 membrane, 304 stainless steel tube, or PFA tube) and a 304 stainless steel shell.

Artificial flue gas (a mixture of compressed air and water vapor) was prepared by bubbling dry air into a steam generator. A mass flow controller (MQV0050, Azbil, Dalian, China) was used to measure the flowrate of dry air. The power of the steam generator was regulated to control the temperature of the artificial flue gas. An electric heater was used to control the relative humidity of the flue gas. Humidity (HMT337, Vaisala, Finland), temperature (MIK-P202, Asmik, China), and pressure transmitters (MIK-P300, Asmik, China) were installed near the inlet and outlet of the membrane condenser to monitor the humidity,

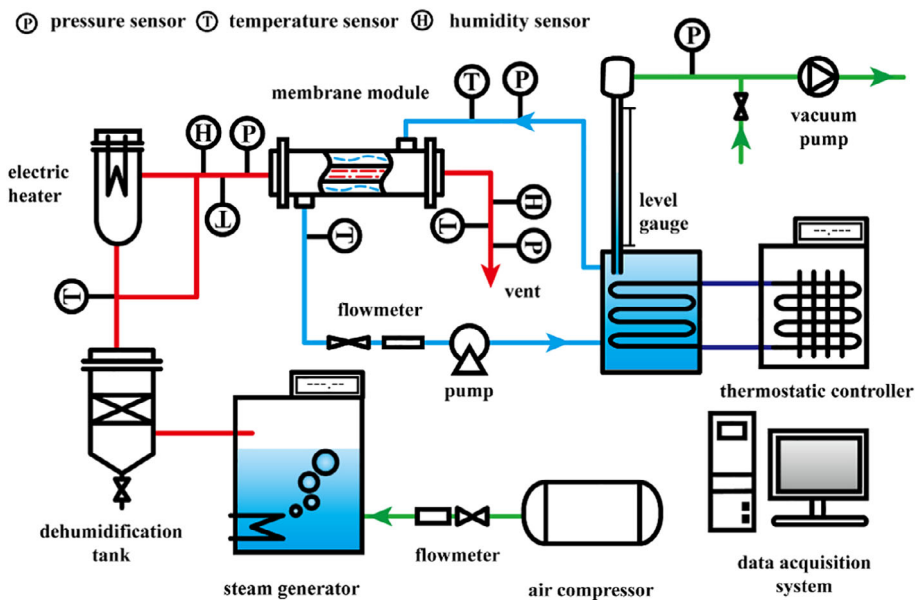**FIGURE 2**   Schematic of the experimental setup [Colour figure can be viewed at wileyonlinelibrary.com]

TABLE 3   Operational parameters applied in this work

Parameter	Value(s)
Air flowrate (SLM, 20°C, 101.325 kPa)	3, 6, 9, 12, 15
Flue gas temperature (°C)	50, 55, 60, 65, 70
Cooling water flowrate (L·min⁻¹)	0.06, 0.2, 0.4, 0.6, 0.8
Cooling water temperature (°C)	10, 15, 20, 25, 30
Relative humidity (%)	100
Transmembrane pressure difference (kPa)	2, 10, 15, 20

temperature, and pressure of the artificial flue gas, respectively. The pipes, tanks, and the outside of the condenser were wrapped with rubber plastic materials to curb heat exchange with the environment.

Cooling water was circulated on the shell side of the condenser, whereas the flue gas flowed countercurrently in the tube. The cooling water temperature was controlled using a chiller. The cooling water flowrate was measured using a glass rotameter. A slight negative pressure (−20 kPa) was provided by the vacuum pump maintained on the circulating water side of the experimental setup for the condensate permeating through the membrane. The volume change of the cooling water was monitored using the level gage installed on the water tank. Once they reached stable values, all operational parameters (i.e., flowrate, temperature, humidity, and pressure) were recorded using the data acquisition system (Nanjing Saint Recovery Technology Co., Ltd., China) for 15 minutes at an interval of 1 minute. No gas bubbles were observed in the circulating water for all experiments, indicating that the TMC has excellent selectivity toward condensable gas.

The uncertainties for the measurements were: volumetric change ± 1.7%, gas flowrate ± 1%, gas side temperature ± 0.5%, water flowrate ±1.5%, water side temperature ± 0.5%, humidity ±1%, and pressure ± 0.1%.

3 | THEORY

3.1 | Heat and mass transfer processes

The condensing heat transfer of pure water vapor and water vapor containing a small amount of noncondensable gases has been extensively researched.[41] However, the volumetric percentage of noncondensable gases is more than 80% for the desulfurated flue gas. The heat transfer process for flue gas that contains predominantly noncondensable gases is very different: with the increasing volumetric percentage of noncondensable gases, the thermal resistance from the noncondensable gas boundary layer, rather than the condensate film, gradually dominates the heat transfer process.

According to Colburn-Hougen's theory,[42] the heat and mass transfer mechanism can be simply illustrated in Figure 3. The total heat (Q_{total}) in condensation process includes the sensible heat (Q_s) and latent heat (Q_l). The former is caused by the flue gas forced convection, and the latter is released by condensation of the vapor. As the flue gas flows in the tubular heat exchange materials, the water vapor in the gas bulk diffuses and condenses on the cold surface of the tube wall. Then, a condensate film is formed on the surface of the tube wall, and the noncondensable gases generate the gas boundary layer between the condensate film and gas bulk.[43] The convective heat and mass
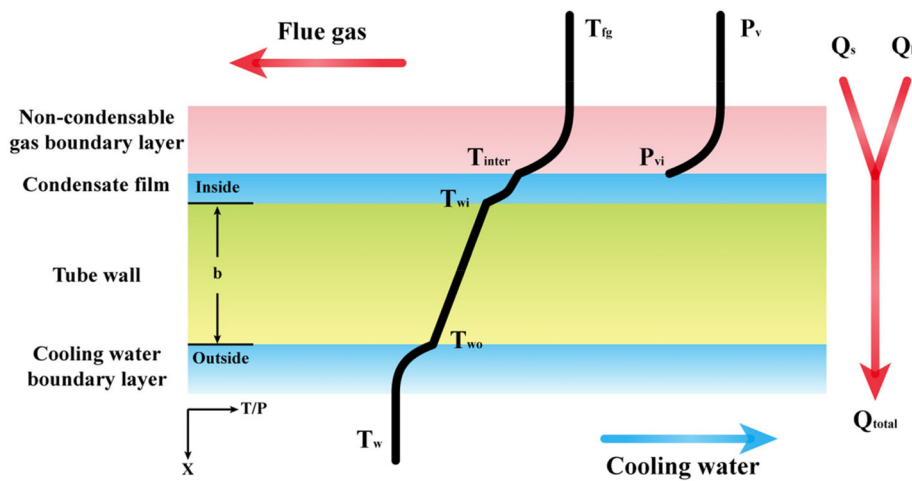
FIGURE 3 Heat and mass transfer in the flue gas condensation process [Colour figure can be viewed at wileyonlinelibrary.com]

transfer occur in the noncondensable gas boundary layer. The temperature difference and vapor partial pressure difference between the gas bulk and interface are the driving forces of heat and mass transfer. Condensation occurs at the interface between the noncondensable gases and condensate. Then, the total heat transfers to the cooling water side through the condensate film, tube wall, and cooling water boundary layer.

The heat and mass transfer mechanisms for dense and porous heat exchange materials are different. Figure 4 shows the schematics of flue gas condensation using dense and porous heat exchange materials. Vapor condensation on the dense surface mostly follows the principle of filmwise condensation where the condensate film may deteriorate the heat and mass transfer. For the ceramic membrane-based flue gas condenser, the condensate can be continuously evacuated to the cooling-water side through membrane pores with the aid of the transmembrane pressure difference. The pores are clogged by the condensate,[30] and other noncondensable gases such as SO_2, NO_x, and CO_2 are prevented from passing through the membrane. The thermal resistance caused by the condensate film is eliminated as no condensed water accumulation occurs on the tube wall.[27] The mass transfer inside the membranes also contributes to the total heat transfer. In addition, capillary condensation, which occurs in the pores and displays excellent gas permeability and selectivity, is a significant transport mechanism in membrane condensers.[4,26,27] The Kelvin equation is used to describe capillary condensation:

$$ln\frac{p}{P_0} = -\frac{2\sigma M cos\theta}{\rho R T r_p} \quad (1)$$

where P is the capillary condensation pressure (Pa), P_0 is the saturated vapor pressure for a planar interface (Pa), σ
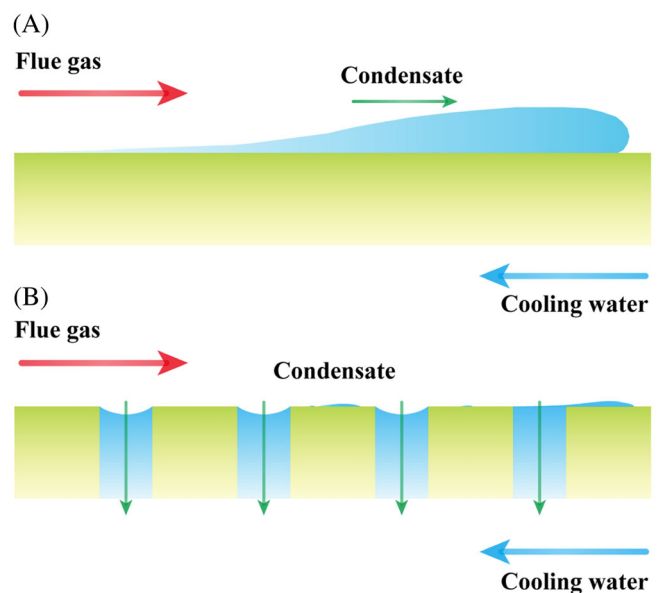

FIGURE 4 Flue gas condenser configurations using A, dense materials and B, porous materials [Colour figure can be viewed at wileyonlinelibrary.com]

is the surface tension ($N \cdot m^{-1}$), M is the molar mass of the condensate ($kg \cdot mol^{-1}$), θ is the contact angle (deg), ρ is the condensate density ($kg \cdot m^{-3}$), R is the gas constant ($J \cdot mol^{-1} \cdot K^{-1}$), T is the temperature (K), and r_p is the pore radius (m).

3.2 | Heat transfer calculation

The total heat flow (Q_t) is calculated using the following expression:[30]

$$Q_t = C_w \dot{m}_{w,in} \Delta T + \dot{m}_c h(T) \quad (2)$$

where C_w is the specific heat capacity of water (kJ·kg^{-1}·K^{-1}), $h(T)$ is the specific enthalpy of water (kJ·kg^{-1}) at temperature T, ΔT is the temperature change of the cooling water (K), $\dot{m}_{w,in}$ is the mass flowrate of the inlet cooling water (kg·h^{-1}), and $\dot{m}_c$ is the condensate transfer rate (kg·h^{-1}).

The overall heat transfer coefficient is a complicated function of tube dimensions, material thermal conductivities, fluid properties, flowrates, and fouling thermal resistances.[17] Taking the internal surface of the heat exchange tube as a reference, the overall heat transfer coefficient (K_i) can be calculated as

$$K_i = \frac{Q_t}{A_i \Delta T_m} \tag{3}$$

where A_i is the effective internal surface area of the heat exchange tube (m^2), and ΔT_m is the logarithmic mean temperature difference (LMTD) (K) between the flue gas and cooling water, which is given as follows:[28,44]

$$\Delta T_m = \frac{(T_{fg,in} - T_{w,out}) - (T_{fg,out} - T_{w,in})}{\ln\left(\frac{T_{fg,in} - T_{w,out}}{T_{fg,out} - T_{w,in}}\right)} \tag{4}$$

where $T_{fg,in}$, $T_{fg,out}$, $T_{w,in}$, and $T_{w,out}$ are the temperatures (K) of the inlet flue gas, outlet flue gas, inlet cooling water, and outlet cooling water, respectively.

The resistance-in-series model[31] is used to describe the heat transfer process of membrane condensation:

$$K_i = \frac{1}{\frac{1}{\alpha_i} + \frac{A_i}{2\pi\lambda_t L}ln\frac{r_o}{r_i} + \frac{A_i}{A_o}\frac{1}{\alpha_o}}, K_i A_i = \frac{1}{\sum R_{th}} \tag{5}$$

where r_i and r_o are the inner and outer radius of the heat exchange tube (m); L is the length of tube (m); A_i and A_o are the internal and external surface area of the heat exchange tube (m^2); λ_t is the tube wall thermal conductivity (W·m^{-1}·K^{-1}); α_i is the total heat transfer coefficient of flue gas side (including both convection and condensation) (W·m^{-2}·K^{-1}); α_o is the convective heat transfer coefficient in the cooling water side (W·m^{-2}·K^{-1}); R_{th} refers to thermal resistance (K·W^{-1}). The fouling thermal resistances were neglected in the experimental conditions.

The thermal resistance in the tube wall (R_t) can be expressed as

$$R_t = \frac{1}{2\pi\lambda_t L}ln\frac{r_o}{r_i} \tag{6}$$

where the thermal conductivity (λ_t) for porous membrane wetted by water is determined by

$$\lambda_t = (1-\gamma)\lambda_m + \gamma\lambda_w \tag{7}$$

where γ is the porosity of the membrane, λ_m and λ_w are the thermal conductivities (W·m^{-1}·K^{-1}) of the membrane material and water, respectively. The porosities of the SiC and Al$_2$O$_3$ tubes, which were determined using Archimedes' method, are 46% and 36%, respectively.

The thermal resistance in the cooling water boundary layer (R_w) can be calculated as

$$R_w = \frac{1}{\alpha_o A_o} \tag{8}$$

The flowrate of the recovered water is negligible with respect to that of the cooling water[45] (the difference in this work is two orders of magnitude). The water flow in our experiment is in the laminar flow state, and the convective heat transfer coefficient at the wall-water interface (α_o) can be estimated using the Sieder-Tate correlation developed at constant flowrate.[46,47]

$$\alpha_o = \frac{\lambda_w Nu}{d_e} = 1.86 \times \frac{\lambda_w}{d_e}\left(RePr\frac{d_e}{L}\right)^{\frac{1}{3}}\left(\frac{\mu}{\mu_w}\right)^{0.14} \tag{9}$$

where d_e is the equivalent diameter (m), Nu is the Nusselt number, Pr is the Prandtl number, Re is the Reynolds number, L is the tube length (m), and μ is the viscosity (Pa·s).

The thermal resistance in the noncondensable gas boundary layer (R_{fg}) can be determined using the following expression:

$$R_{fg} = \frac{1}{K_i A_i} - R_t - R_w \tag{10}$$

3.3 | Water recovery performance evaluation

Water flux and water recovery efficiency are crucial criteria for assessing water recovery performance. The water flux of ceramic membranes (J_w) can be determined as follows:

$$J_w = \frac{\dot{m}_{w,out} - \dot{m}_{w,in}}{A_i} = \frac{\rho \Delta v}{2\pi r_i L \Delta t} \tag{11}$$

where $\dot{m}_{w,in}$ and $\dot{m}_{w,out}$ are the mass flowrates of the inlet and outlet cooling water (kg·h^{-1}), and Δv is the volumetric change (m^3) of the cooling water during the period of time Δt (h).

The mass transfer mechanisms of porous and dense materials are different. For the comparable experiments of water recovery performance in Sections 4.3.2 and 4.3.3, the water flux (J_v) and water recovery efficiency (η_v) of the four materials are determined by the flue gas parameters:

$$J_v = \frac{\dot{m}_{vap,in} - \dot{m}_{vap,out}}{A_i} = \frac{\dot{m}_{air}(x_{in} - x_{out})}{2\pi r_i L} \qquad (12)$$

$$\eta_v = \frac{\dot{m}_{vap,in} - \dot{m}_{vap,out}}{\dot{m}_{vap,in}} \times 100\% = \frac{x_{in} - x_{out}}{x_{in}} \times 100\% \qquad (13)$$

where $\dot{m}_{vap,in}$, $\dot{m}_{vap,out}$, $\dot{m}_{air}$ are the mass flowrates of inlet water vapors, outlet water vapors, and dry air ($kg \cdot h^{-1}$), respectively. x is the mixing ratio (mass of water vapor/mass of dry gas), which is obtained from the Humidity Calculator software (Vaisala, Finland).

4 | RESULTS AND DISCUSSION

4.1 | Energy balance and uncertainty analysis

Energy balance between the hot and cold fluids of a condenser is the essential information required to assess the reliability of the experimental system.[48] A series of condensation experiments of the four materials was conducted under corresponding operational parameters. The energy changes of the flue gas side (q_g) and cooling water side (q_w) can be calculated using the following equations:

$$q_g = \frac{\dot{m}_{fg,in} h_{fg,in} - \dot{m}_{fg,out} h_{fg,out}}{A_i} \qquad (14)$$

$$q_w = \frac{C_w \dot{m}_{w,in} \Delta T + \dot{m}_c h(T)}{A_i} \qquad (15)$$

where $\dot{m}_{fg,in}$ and $\dot{m}_{fg,out}$ are the mass flowrates ($kg \cdot h^{-1}$) of the inlet and outlet flue gases, respectively, and h is the specific enthalpy ($kJ \cdot kg^{-1}$). As shown in Figure 5, the deviations between all of the q_g and q_w values fall within ±10%. These results indicate the good reliability of the experimental system.

According to reference,[17,43] the uncertainties of the experimental results were calculated to analyze the experimental errors. The maximum uncertainties of the overall heat transfer coefficient (K_i), water flux (J_v), and water recovery efficiency (η_v) are estimated to be 3.37%, 4.43%, and 3.61%, respectively.
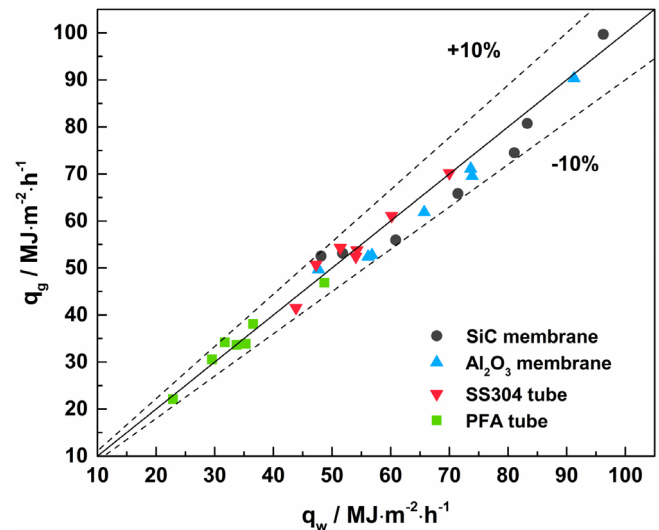

FIGURE 5 Energy balance of the experimental system [Colour figure can be viewed at wileyonlinelibrary.com]

4.2 | Heat transfer performance

Condensation experiments using different heat exchange materials were performed under consistent operational parameters in Table 3. The heat transfer performance of condensers can be evaluated using the overall heat transfer coefficient (K_i). As depicted in Figure 6, the sequence of overall heat transfer coefficients for different heat exchange materials is as follows: SiC membrane > Al_2O_3 membrane > 304 stainless steel > PFA. Compared with other materials, the SiC membrane achieves a higher overall heat transfer coefficient at a lower temperature difference under consistent operational parameters. The overall heat transfer coefficients of the SiC membrane vary from 297.1 to 730.2 $W \cdot m^{-2} \cdot K^{-1}$, which are 5%-16%, 8%-19%, and 35%-137% higher than those of the Al_2O_3 membrane, 304 stainless steel, and PFA, respectively. Owing to its porous structure and high heat conductivity, the SiC membrane exhibits a superior heat transfer performance. In contrast, poor heat conducting performance (0.26 $W \cdot m^{-1} \cdot K^{-1}$) weakens heat transfer across the PFA tube, even though it has a thinner tube wall. The influence of mass transfer on the temperature distribution in the membrane can be ignored, and the heat conduction is the main heat transfer inside the tubular membrane.[49] Figure 7 shows the thermal-conduction resistances of the four tubes. The thermal resistance of the Al_2O_3 tube is about 15 times higher than that of SiC tube. Thus, the Al_2O_3 membrane shows a lower heat transfer performance than the SiC membrane. In fact, the structure of the SiC membrane used in our experiment is not optimal. The heat transfer performance of SiC membranes can be further enhanced by reducing the total porosity.[50]

FIGURE 6 Heat transfer performance of different heat exchange materials. (Typical experimental conditions: air flowrate, 9 SLM; flue gas temperature, 60°C; cooling water flowrate, 0.4 L·min⁻¹; cooling water temperature, 15°C; transmembrane pressure difference, 20 kPa; A, flue gas temperature, 50°C–70°C; B, air flowrate, 3-15 SLM; C, cooling water temperature, 30°C–10°C; D, cooling water flowrate, 0.06-0.8 L·min⁻¹) [Colour figure can be viewed at wileyonlinelibrary.com]
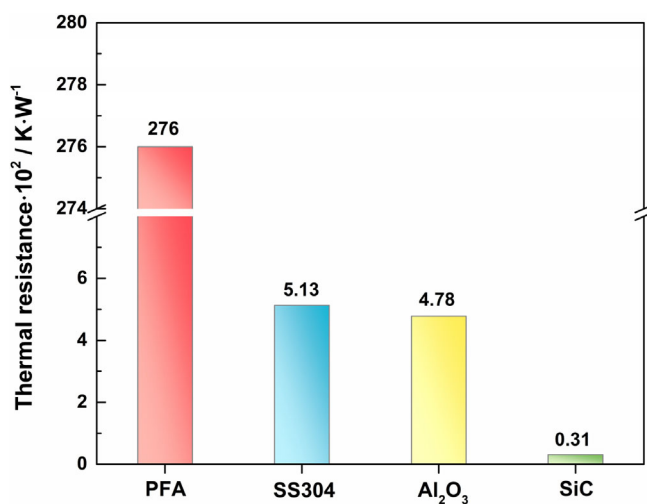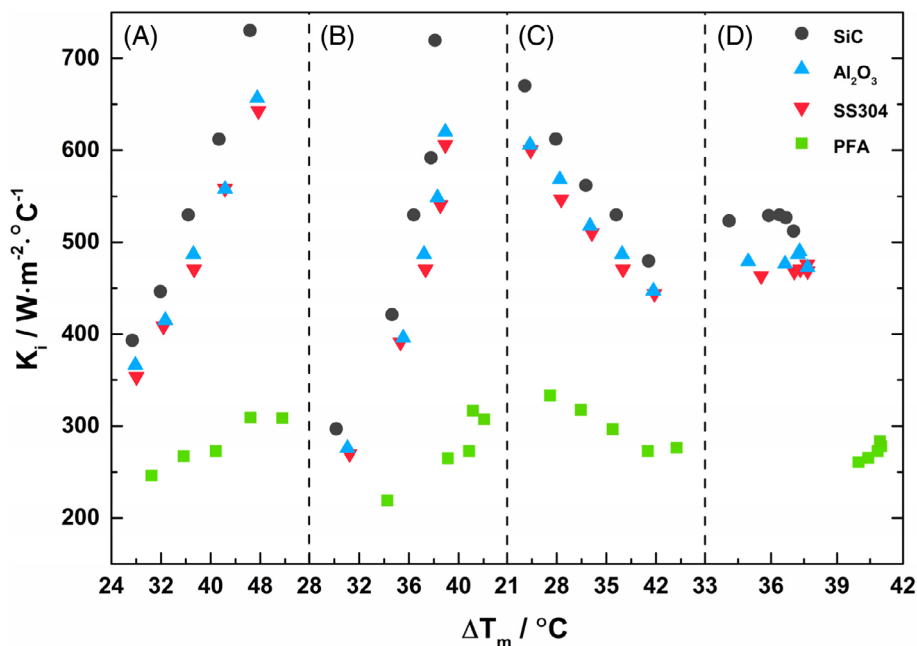

FIGURE 7 Thermal resistance of different tubular materials [Colour figure can be viewed at wileyonlinelibrary.com]

Porous ceramic membranes exhibit higher heat transfer performance than conventional dense materials. However, the overall heat transfer coefficient of the tubular Al_2O_3 membrane is at maximum 4% higher than that of the 304 stainless steel tube, which is slightly different from the results of Bao et al.[26] This distinction can be explained by several reasons. First, the difference in heat transfer performance between porous membranes and dense materials depends on the amount and flow state of the condensate on the gas side. The heat exchange tube used in this experiment is not long enough, resulting in insufficient heat exchange and a thin condensate boundary layer. The advantages of a porous structure cannot be fully reflected. In addition, the flue gas velocity in this experiment (1.4-7.1 m·s⁻¹) is much higher than that in Bao's experiment (0.5 m·s⁻¹). The condensate is quickly removed from the test section under the action of a huge shear force at the gas-liquid interface[51] and could not be accumulated on the tube wall in time. Thus, the 304 stainless steel tube exhibits good heat transfer performance.

Finally, capillary condensation is a significant transport mechanism of ceramic membranes. When the condensable gas component is determined, a relationship exists among the relative pressure (the ratio of the capillary condensation pressure to the plane saturated vapor pressure), pore size, and flue gas temperature, as illustrated in Figure 8. The relative pressure significantly increases as the pore size rises from 2 to 100 nm. When the membrane pore size is larger than 100 nm, the dimensionless relative pressure is approximately 1, indicating that capillary condensation will never occur. Bao's experiment is based on the nanoporous Al_2O_3 membranes with pore sizes of 6-8 nm, whereas the average pore size of the Al_2O_3 membrane used in this work is 0.4 μm. Consequently, the difference in heat transfer performance between the tubular Al_2O_3 membrane and 304 stainless steel tube is not obvious in this study.

4.3 | Effects of operational parameters on water recovery performance

4.3.1 | Transmembrane pressure difference

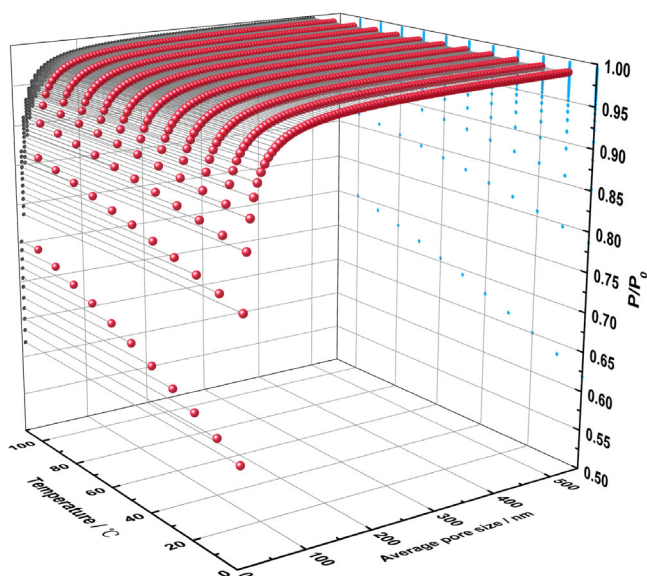The transmembrane pressure difference is the driving force for the condensate permeating through ceramic

FIGURE 8 Effects of pore size and temperature on the capillary condensation of water vapor [Colour figure can be viewed at wileyonlinelibrary.com]

FIGURE 9 Water flux as a function of transmembrane pressure difference. (Experimental conditions: air flowrate, 9 SLM; flue gas temperature, 60°C; cooling water flowrate, 0.4 L·min^{-1}; cooling water temperature, 15°C) [Colour figure can be viewed at wileyonlinelibrary.com]

membranes. Figure 9 shows the influence of transmembrane pressure difference on the water flux of ceramic membranes. The SiC membrane exhibits a higher water flux than the Al_2O_3 membrane. As the transmembrane pressure difference increased from 2 to 20 kPa, the water flux of the SiC membrane remained constant at 25 kg·m^{-2}·h^{-1}; however, the water flux of the Al_2O_3 membrane increased from 11.2 to 23.5 kg·m^{-2}·h^{-1} and then remained constant. In comparison with Al_2O_3 membrane, SiC membrane shows high hydrophilicity, which provides opportunities for SiC membrane to effectively and swiftly permeate water.[36] Pure water permeabilities of the SiC and Al_2O_3 membranes used in this study were measured using a home-made cross-flow filtration device at a transmembrane pressure of 0.1 MPa, which are 16 000 and 3000 L·m^{-2}·h^{-1}·bar^{-1}, respectively. The mass transfer resistances determined by Darcy's law[52] of the two ceramic membranes are 0.22×10^{-11} and 1.18×10^{-11} m^{-1}, respectively. Membrane condensation can be regarded as the process of condensation followed permeation. As we know, water flux of membrane is proportional to transmembrane pressure difference. Water condensed via membrane condenser cannot be completely recovered if the permeability of membrane is poor and/or the transmembrane pressure difference is low. Owing to poor permeability of the Al_2O_3 membrane, the water flux of the Al_2O_3 membrane is far below that of the SiC membrane under low transmembrane pressure difference. As depicted in Figure 9, the water flux does not change at high transmembrane pressure difference,
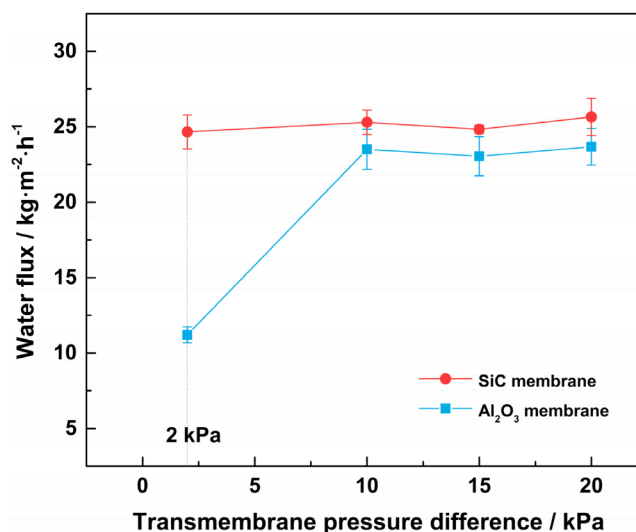
suggesting that the condensate on the membrane surface is completely eliminated. The following experiments were conducted at a transmembrane pressure difference of 20 kPa to ensure no accumulation of condensate on the surface of ceramic membranes.

In addition, compared with the mesoporous ceramic membranes used in some studies,[27,30,53] the macroporous ceramic membranes used in this experiment can eliminate a condensate film at a lower transmembrane pressure difference (below 20 kPa) because of the higher water permeability produced by large pores. The result indicates that ceramic membranes with superior permeability should be developed for moisture recovery to reduce energy consumption.

4.3.2 | Flue-gas-side operational parameters

Figure 10 illustrates the effects of flue-gas-side operational parameters on water recovery performance. Porous ceramic membranes show higher water recovery performance than conventional dense materials, and the SiC membrane exhibits superior performance than the Al_2O_3 membrane. With increasing air flowrate and flue gas temperature, the gap of water recovery performance between these materials increases, suggesting that the thermal resistance from the material rather than the boundary layer becomes increasingly dominant in the heat and mass transfer processes.
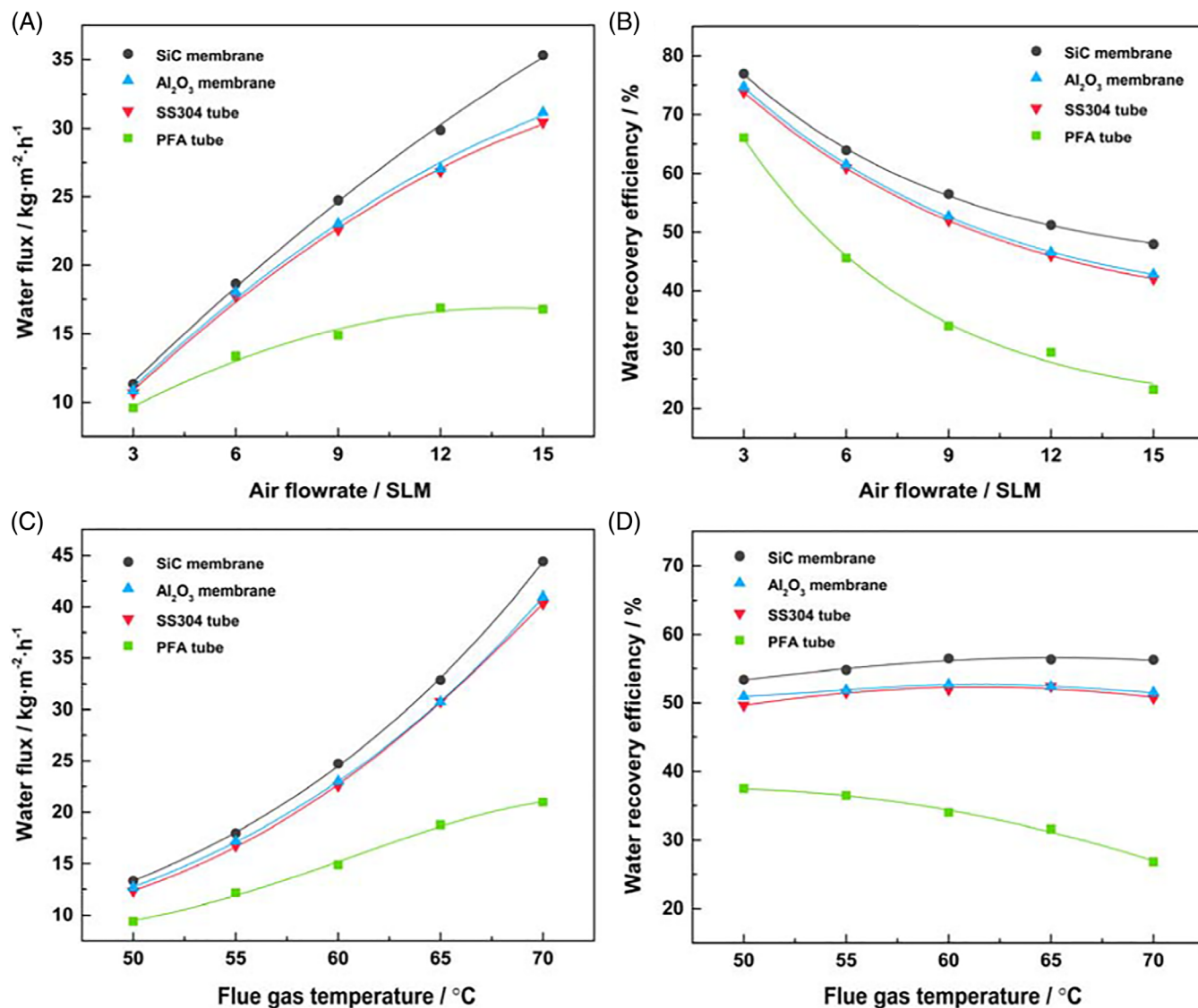
FIGURE 10 Water flux and recovery efficiency as functions of air flowrate A and B, and flue gas temperature C and D. (Typical experimental conditions: air flowrate, 9 SLM; flue gas temperature, 60°C; cooling water flowrate, 0.4 L·min^{-1}; cooling water temperature, 15°C; transmembrane pressure difference, 20 kPa) [Colour figure can be viewed at wileyonlinelibrary.com]

Figure 10A, B depicts the influence of air flowrate on water recovery performance. The air volume flowrate[16] in the standard state (101.325 kPa, 20°C) is used to represent the flue gas flowrate as the moisture content and volume flowrate of saturated wet flue gas vary with the experimental temperature. With increasing air flowrate, the water flux drastically increases. Taking the SiC membrane as an example, the water flux increased by 212% (from 11.33 to 35.32 kg·m^{-2}·h^{-1}) when the air flowrate increased from 3 to 15 SLM. The high velocity of the flue gas increases the turbulence on the gas side and enhances the heat transfer process. The resistance of water vapor diffusing through the noncondensable gas boundary layer to the membrane surface is reduced

with the increasing flue gas velocity. Simultaneously, more water vapor enters the membrane condenser at a higher air flowrate. Consequently, a higher permeate flux of water can be achieved. In contrast, the water recovery efficiency decreases with the increasing air flowrate. As the air flowrate increased from 3 to 15 SLM, the water recovery efficiency of the SiC membrane decreased from 76.9% to 47.9%. The residence time between the water vapor and condenser plays an important role in water recovery efficiency. With the increasing flue gas velocity, the residence time of flue gas is shortened. Large amounts of unrecovered water vapor within the outlet gas results in low condensation efficiency. In short, enhancing condensing heat transfer

and increasing the residence time of flue gas are necessary for moisture recovery, for example, baffle plates are extensively used in heat exchangers.[54] However, the pressure loss of condensers should be considered to prevent the pressure change of the flue gas from affecting the normal operation of other pieces of equipment in power plants.

Figure 10C, D describes the influence of flue gas temperature on water recovery performance. The water flux across the membrane significantly increases with the increasing flue gas temperature. Taking the SiC membrane as an example, the water flux increased by 233% (from 13.33 to 44.43 $kg \cdot m^{-2} \cdot h^{-1}$) when the flue gas temperature increased from 50°C to 70°C. The result indicates that the flue gas temperature has an important effect on water flux. The flue gas condensation process is enhanced because of the improved heat transfer driving force (i.e., the temperature difference between the gas bulk and the surface of the tube wall).[44] In addition, the increase in flue gas temperature generates a higher partial pressure of the vapor when the relative humidity of the flue gas is unchanged. When the flue gas temperature increased from 50°C to 70°C, the water vapor partial pressure in the flue gas varied from 12.38 to 31.25 kPa, with an increase of 152%. The higher mass transfer driving force resulted from the higher vapor partial pressure difference between the gas bulk and the membrane surface effectively drives the condensation process. The changes in the water recovery efficiency of different materials show interesting trends. As the flue gas temperature increased from 50°C to 70°C, the water recovery efficiency of the SiC membrane slightly improved from 53.4% to 56.5% and then declined to 56.3%. However, the water recovery efficiency of the PFA tube decreased from 37.5% to 26.8% within the gas temperature range. As we know, the moisture content, which is relevant to inlet gas temperature, is the main factor affecting the water recovery performance.[49] Both the water flux and moisture content of the inlet saturated flue gas rise with the increasing gas temperature. Water recovery efficiency increases when the measured water flux increases faster than the inlet gas moisture content. However, when the moisture content of the inlet gas is such high that the condenser cannot effectively recover the water, the water recovery efficiency declines. As a result, the changes in water recovery efficiency exhibit different trends.

4.3.3 | Cooling-water-side operational parameters

Figure 11 shows the variations in water recovery performance with cooling-water-side operational parameters.

Consistent with the results in Section 4.3.2, the sequence of water recovery performance for different heat exchange materials is as follows: SiC membrane > Al_2O_3 membrane > 304 stainless steel > PFA.

Figure 11A, B depicts the influence of the flowrate of cooling water on water recovery performance. As the cooling water flowrate increases, water recovery performance slightly improves. Taking the SiC membrane as an example, when the cooling water flowrate increased from 0.06 to 0.8 $L \cdot min^{-1}$, the water flux increased by 8% (from 22.94 to 24.77 $kg \cdot m^{-2} \cdot h^{-1}$). Meanwhile, the water recovery efficiency increased from 52.5% to 56.5%. Compared with the flowrate of flue gas, the cooling water flowrate exhibits insignificant effects on the water recovery performance,[45] suggesting that the flue gas condensation process is significantly affected by the magnitudes of the thermal resistance in the noncondensable gas boundary layer, rather than in the water boundary layer, relative to the total thermal resistance. The ratio of the cooling water flowrate to the flue gas flowrate is an important parameter for assessing the efficiency of condensers. Thus, under the premise of ensuring water recovery efficiency, the cooling water flowrate should be reduced to cut down the energy consumption of the fluid conveying device.

Figure 11C, D describes the influence of cooling water temperature on water recovery performance. As the cooling water temperature increases, both water flux and water recovery efficiency gradually decrease. Taking the SiC membrane as an example, when the cooling water temperature increased from 10°C to 30°C, the water flux decreased by 24% (from 25.19 to 20.29 $kg \cdot m^{-2} \cdot h^{-1}$). Meanwhile, the water recovery efficiency decreased from 57.7% to 46.5%. The decrease in temperature difference between the cold and hot fluids deteriorates the heat and mass transfer. Obviously, the water recovery performance could be significantly enhanced using low-temperature water. However, the temperature of cooling water is generally higher than 25°C in most thermal power plants.[34] Low-temperature water would increase the operating costs of power plants. Air-cooling is reportedly feasible for flue gas dehydration.[55] Although air-cooling is not highly efficient because of the lower specific heat capacity of air than water, air is available and inexhaustible.

4.4 | Heat transfer enhancement

The heat transfer enhancement of heat exchangers generally includes three aspects: expanding the heat transfer area (A), increasing the heat transfer temperature difference (ΔT_m), and improving the heat transfer coefficient

(K). For a designated thermal power plant, the equipment space, flue gas temperature, and cooling water temperature are determined. Thus, improving the heat transfer coefficient (i.e., reducing the total thermal resistance) is the most suitable method to enhance the heat transfer performance.

The total thermal resistance in the flue gas condensation process can be regarded as the superposition of various thermal resistances. As analyzed in Section 3, thermal resistances in flue gas condensers originate from four aspects: noncondensable gas boundary layer, condensate film, tube wall, and cooling water boundary layer. Porous ceramic membranes can completely eliminate the thermal resistance of the condensate film. Furthermore, the thermal resistance in the tube wall can be reduced using high thermal conductivity material (e.g., SiC) as the membrane material. Figure 12 shows the thermal resistance distribution of the SiC membrane condenser under typical experimental conditions in this experiment. The thermal resistance in the tube wall is significantly lower than that in the boundary layers. Although the Reynolds numbers of flue gas (1055-5277) are much higher than those of water (39-522), the thermal resistance in the gas boundary layer is still 2.2-6.8 times higher than that in the water boundary layer, indicating that the thermal resistance in the gas boundary layer is the key thermal resistance. Hence, heat transfer enhancement by reducing the thermal resistance in the noncondensable gas boundary layer should be investigated in the future.
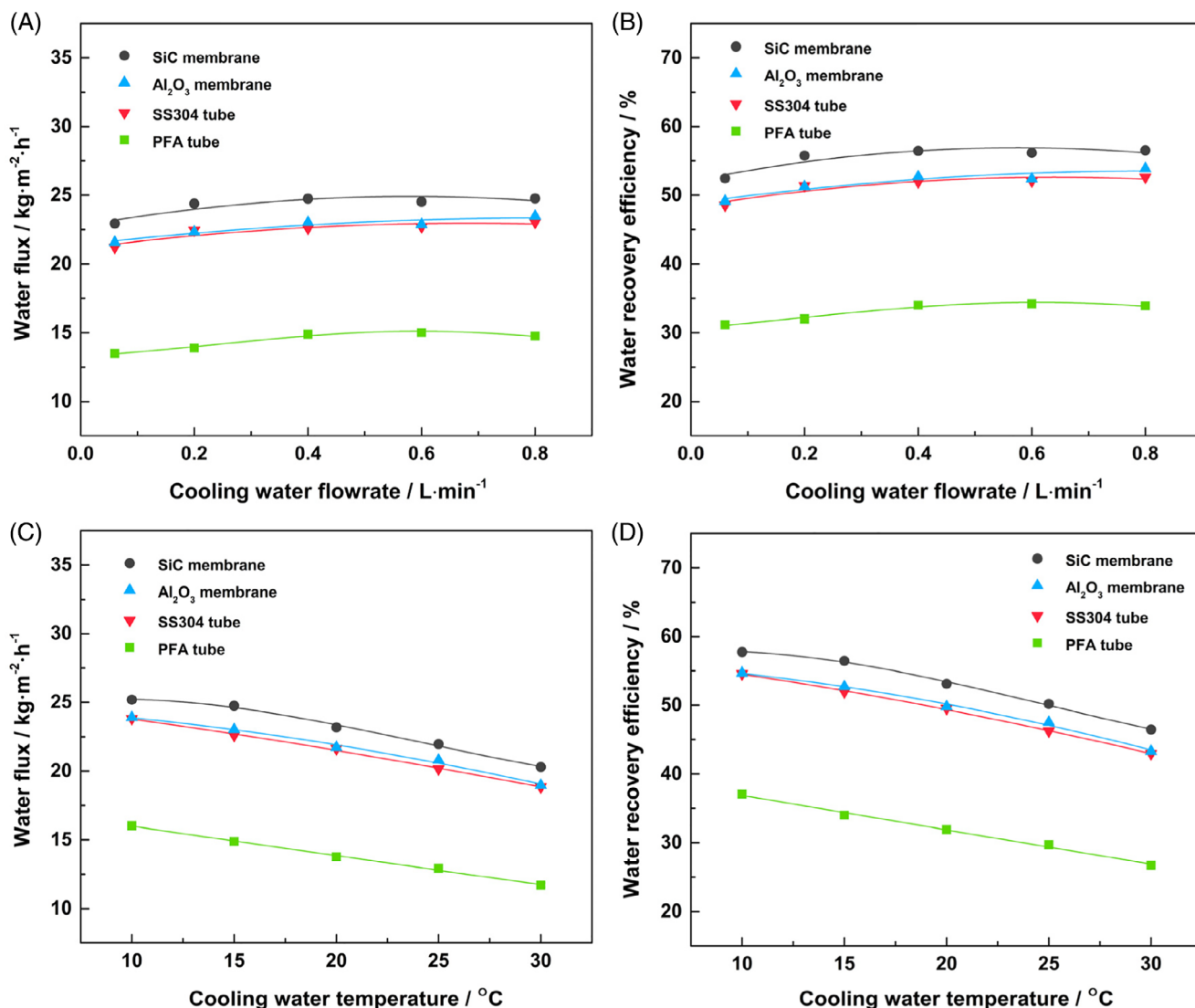

FIGURE 11 Water flux and recovery efficiency as functions of cooling water flowrate A and B, and cooling water temperature C and D. (Typical experimental conditions: air flowrate, 9 SLM; flue gas temperature, 60°C; cooling water flowrate, 0.4 L·min^{-1}; cooling water temperature, 15°C; transmembrane pressure difference, 20 kPa) [Colour figure can be viewed at wileyonlinelibrary.com]

(A)

(B)

FIGURE 12 Thermal resistance distribution of the SiC membrane condenser under typical experimental conditions. (Air flowrate, 3-15 SLM; flue gas temperature, 50°C–70°C; cooling water flowrate, 0.4 L·min⁻¹; cooling water temperature, 15°C; transmembrane pressure difference, 20 kPa) [Colour figure can be viewed at wileyonlinelibrary.com]
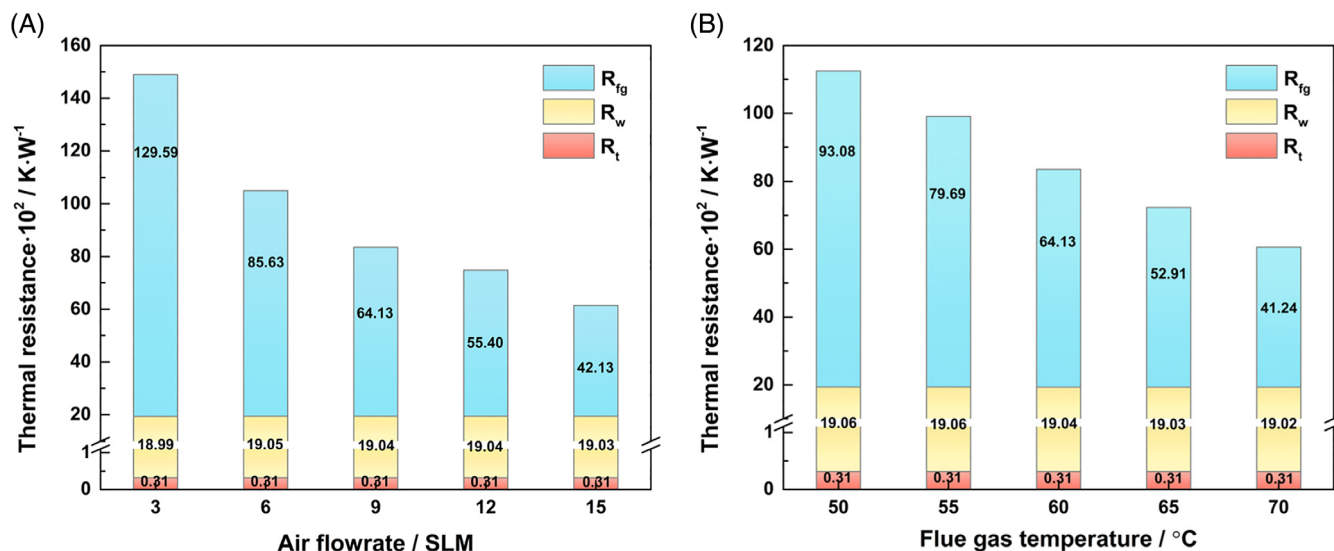
5 | CONCLUSIONS

Herein, for the first time, we report a tubular SiC membrane for water and heat recovery from high-moisture flue gas. The heat transfer and water recovery performances of a tubular SiC membrane were compared with those of the tubular Al_2O_3 membrane, 304 stainless steel tube, and PFA tube in terms of several important operational parameters (i.e., air flowrate, flue gas temperature, cooling water flowrate, cooling water temperature, and transmembrane pressure difference). The following conclusions are drawn from this work.

1. Porous ceramic membranes show better heat transfer performance than conventional dense materials. The overall heat transfer coefficients of the SiC membrane are 5%-16% higher than those of the Al_2O_3 membrane, suggesting that the SiC membrane is more suitable for flue gas condensation. Moreover, the sequence of water recovery performance for different heat exchange materials is as follows: SiC membrane > Al_2O_3 membrane >304 stainless steel > PFA. Water flux of 11.3-44.4 kg·m⁻²·h⁻¹ and water recovery efficiency of 46.5%-76.9% were achieved using the SiC membrane.

2. The transmembrane pressure difference has a little effect on water flux when the condensate permeation rate is higher than the flue gas condensation rate. Increasing the flue gas flowrate improves the water flux but reduces the water recovery efficiency. The increase in flue gas temperature significantly enhances the heat and mass transfer process,

generating improved water flux. Nevertheless, the flue gas temperature only slightly affects water recovery efficiency. As the flowrate of cooling water increases, water recovery performance slightly improves. Water flux and water recovery efficiency significantly reduce as the cooling water temperature increases.

3. The thermal resistance in the noncondensable gas boundary layer of SiC membrane condensers is two orders of magnitude larger than that in the tube wall and 2.2-6.8 times higher than that in the water boundary layer. Thus, the convection-condensing heat transfer on the gas side should be enhanced in a further study.

NOMENCLATURE

P	capillary condensation pressure (Pa)
P_0	saturated vapor pressure for a planar interface (Pa)
M	molar mass of the condensate (kg·mol⁻¹)
R	gas constant (J·mol⁻¹·K⁻¹)
T	temperature (K)
r_p	pore radius (m)
C_w	specific heat capacity of water (kJ·kg⁻¹·K⁻¹)
h	specific enthalpy (kJ·kg⁻¹)

ΔT temperature change of the cooling water (K)
$\dot{m}$ mass flow rate (kg·h^{-1})
$\dot{m}_c$ condensate transfer rate (kg·h^{-1}).
Q_t total heat flow (kJ·h^{-1})
A_i effective internal surface area of the heat exchange tube (m^2)
ΔT_m logarithmic mean temperature difference (K)
K_i overall heat transfer coefficient (W·m^{-2}·K^{-1})
r radius of the heat exchange tube (m)
R_{th} thermal resistance (K·W^{-1})
d_e equivalent diameter (m)
Nu Nusselt number
Pr Prandtl number
Re Reynolds number
L tube length (m)
Δv volumetric change (m^3)
J water flux (kg·m^{-2}·h^{-1})

GREEK SYMBOLS

σ surface tension (N·m^{-1})
θ contact angle (°)
α heat transfer coefficient (W·m^{-2}·K^{-1})
ρ condensate density (kg·m^{-3})
λ_t tube wall thermal conductivity (W·m^{-1}·K^{-1})
λ_m thermal conductivity of material (W·m^{-1}·K^{-1})
λ_w thermal conductivity of water (W·m^{-1}·K^{-1})
γ porosity of the membrane
μ viscosity (Pa·s)
η_v water recovery efficiency

SUBSCRIPTS

fg   flue gas
w   water
vap   water vapor
in   inlet
out   outlet
i   inner
o   outer
t   tube wall

ORCID

Hong Qi https://orcid.org/0000-0002-2466-8561

REFERENCES

1. Wang D. *Simultaneous Waste Heat and Water Recovery from Power Plant Flue Gases for Advanced Energy Systems, Final Report DE-FE0024092*. Des Plaines, IL: Gas Technology Institute; 2016. https://doi.org/10.2172/1347684.
2. Kim S, Lim Y-I, Lee D, Seo MW, Mun T-Y, Lee J-G. Effects of flue gas recirculation on energy, exergy, environment, and economics in oxy-coal circulating fluidized-bed power plants with CO$_2$ capture. *Int J Energy Res*. 2020;1-14. https://doi.org/10.1002/er.6205.
3. Xu G, Huang S, Yang Y, Wu Y, Zhang K, Xu C. Techno-economic analysis and optimization of the heat recovery of utility boiler flue gas. *Appl Energy*. 2013;112:907-917.
4. Wang D, Bao A, Kunc W, Liss W. Coal power plant flue gas waste heat and water recovery. *Appl Energy*. 2012;91(1):341-348.
5. Ma S, Chai J, Jiao K, Ma L, Zhu S, Wu K. Environmental influence and countermeasures for high humidity flue gas discharging from power plants. *Renew Sustain Energy Rev*. 2017;73:225-235.
6. Judd S, Jefferson B. Membrane for industrial wastewater recovery and re-use. *Filtr*. 2003;40:38-40.
7. Zhuang Y, Gu P, Ouyang L, Chen Z, Liu K. Experimental study of formation mechanism of stack rainout from coal-fired power plant. *China Environ Sci*. 2015;35(3):714-722.
8. Gao D, Li Z, Zhang H, Chen H, Cheng C, Liang K. Moisture and latent heat recovery from flue gas by nonporous organic membranes. *J Clean Prod*. 2019;225:1065-1078.
9. Shen C-H, Chen W-H, Hsu H-W. Co-gasification performance of coal and petroleum coke blends in a pilot-scale pressurized entrained-flow gasifier. *Int J Energy Res*. 2012;36:499-508.
10. Chen C-Y, Chen W-H, Ilham Z. Effects of torrefaction and water washing on the properties and combustion reactivity of various wastes. *Int J Energy Res*. 2020;1-15. https://doi.org/10.1002/er.5458.
11. Gao D, Li Z, Zhang H, Chen H, Wang L, Liu H. The investigation of desulphurization and water recovery from flue gas using ceramic composite membrane. *Int J Energy Res*. 2019;43:1747-1759.
12. Jeong K, Kessen M, Bilirgen H, Levy E. Analytical modeling of water condensation in condensing heat exchanger. *Int J Heat Mass Transf*. 2010;53(11–12):2361-2368.
13. Wang L, He Y, Tang C, Wang Y, Che D. A novel design of rotary regenerative condensing heat exchanger for the dehydration from high humidity flue gas. *Int J Heat Mass Transf*. 2019;131:517-526.
14. Wei M, Zhao X, Fu L, Zhang S. Performance study and application of new coal-fired boiler flue gas heat recovery system. *Appl Energy*. 2017;188:121-129.
15. Xiong Y, Tan H, Wang Y, Xu W, Mikulcic H, Duic N. Pilot-scale study on water and latent heat recovery from flue gas using fluorine plastic heat exchangers. *J Clean Prod*. 2017;161:1416-1422.
16. Kim J, Park A, Kim S, et al. Harnessing clean water from power plant emissions using membrane condenser technology. *ACS Sustain Chem Eng*. 2018;6(5):6425-6433.
17. Chen L, Li Z, Guo Z. Experimental investigation of plastic finned-tube heat exchangers, with emphasis on material thermal conductivity. *Exp Therm Fluid Sci*. 2009;33(5):922-928.
18. Wang Z, Zhang X, Li Z. Evaluation of a flue gas driven open absorption system for heat and water recovery from fossil fuel boilers. *Energy Convers Manag*. 2016;128:57-65.
19. Jamil SR, Wang L, Che D. Techno-economic analysis of a novel hybrid heat pump system to recover waste heat and condensate from the low-temperature boiler exhaust gas. *Int J Energy Res*. 2020;48:3821-3838.
20. Xiao L, Yang M, Zhao S, Yuan W, Huang S. Entropy generation analysis of heat and water recovery from flue gas by transport membrane condenser. *Energy*. 2019;174:835-847.
21. Chen H, Zhou Y, Sun J, et al. An experimental study of membranes for capturing water vapor from flue gas. *J Energy Inst*. 2018;91(3):339-348.

22. Macedonio F, Brunetti A, Barbieri G, Drioli E. Membrane condenser configurations for water recovery from waste gases. *Sep Purif Technol*. 2017;181:60-68.

23. Sijbesma H, Nymeijer K, Marwijk R, Heijboer R, Wessling PJM. Flue gas dehydration using polymer membranes. *J Membr Sci*. 2008;313(1–2):263-276.

24. Cao J, Pan J, Cui Z, Wang Z, Wang X, Drioli E. Improving efficiency of PVDF membranes for recovering water from humidified gas streams through membrane condenser. *Chem Eng Sci*. 2019;210:115234.

25. Wang D. *Advanced Energy and Water Recovery Technology from Low Grade Waste Heat, Final Report DE-EE0003477*. Des Plaines, IL: Gas Technology Institute; 2011. https://doi.org/10.2172/1031483.

26. Bao A, Wang D, Lin C. Nanoporous membrane tube condensing heat transfer enhancement study. *Int J Heat Mass Transf*. 2015;84:456-462.

27. Hu H, Tang G, Niu D. Wettability modified nanoporous ceramic membrane for simultaneous residual heat and condensate recovery. *Sci Rep*. 2016;6:27274.

28. Yang B, Shen G, Chen H, Feng Y, Wang L. Experimental study of condensation heat-transfer and water-recovery process in a micro-porous ceramic membrane tube bundle. *Appl Therm Eng*. 2019;155:354-364.

29. Yang B, Chen H. Heat and water recovery from flue gas: application of micro-porous ceramic membrane tube bundles in gas-fired power plant. *Chem Eng Process*. 2019;137:116-127.

30. Wang T, Yue M, Qi H, Feron P, Zhao S. Transport membrane condenser for water and heat recovery from gaseous streams: performance evaluation. *J Membr Sci*. 2015;484:10-17.

31. Yue M, Zhao S, Feron P, Qi H. Multichannel tubular ceramic membrane for water and heat recovery from waste gas streams. *Ind Eng Chem Res*. 2016;55(9):2615-2622.

32. Meng Q, Cao Y, Huang Y, et al. Effects of process parameters on water and waste heat recovery from flue gas using ceramic ultrafiltration membranes. *Ciesc J*. 2018;69(6):2519-2525.

33. Cao Y, Wang L, Ji C, et al. Pilot-scale application on dissipation of smoke plume from flue gas using ceramic membrane condensers. *Ciesc J*. 2019;70(6):2192-2201.

34. Gao D, Li Z, Zhang H, Zhang J, Chen H, Fu H. Moisture recovery from gas-fired boiler exhaust using membrane module array. *J Clean Prod*. 2019;231:1110-1121.

35. Zhao C, Ji W, Jin P, Zhong Y, Tao W. The influence of surface structure and thermal conductivity of the tube on the condensation heat transfer of R134a and R404A over single horizontal enhanced tubes. *Appl Therm Eng*. 2017;125:1114-1122.

36. Li S, Wei C, Zhou L, Wang P, Li M, Xie Z. Tuning microstructures and separation behaviors of pure silicon carbide membranes. *Ceram Int*. 2019;45(15):18788-18794.

37. Hostasa J, Pabst W, Matejicek J. Thermal conductivity of Al_2O_3–ZrO_2 composite ceramics. *J Am Ceram Soc*. 2011;94(12):4404-4409.

38. Watari K. High thermal conductivity non-oxide ceramics. *J Cerma Soc Jpn*. 2001;109(1):S7-S16.

39. Partridge G. Inorganic materials .5. Ceramic materials possessing high thermal-conductivity. *Adv Mater*. 1992;4(1):51-54.

40. Li Y, Yin J, Wu H, Lu P, Yan Y, Liu X. High thermal conductivity in pressureless densified SiC ceramics with ultra-low contents of additives derived from novel boron-carbon sources. *J Eur Ceram Soc*. 2014;34(10):2591-2595.

41. Che D, Da Y, Zhuang Z. Heat and mass transfer characteristics of simulated high moisture flue gases. *Heat Mass Transf*. 2005;41(3):250-256.

42. Machackova A, Kocich R, Bojko M, Kuncicka L, Polko K. Numerical and experimental investigation of flue gases heat recovery via condensing heat exchanger. *Int J Heat Mass Transf*. 2018;124:1321-1333.

43. Shi X, Che D, Agnew B, Gao J. An investigation of the performance of compact heat exchanger for latent heat recovery from exhaust flue gases. *Int J Heat Mass Transf*. 2011;54(1–3):606-615.

44. Yan S, Cui Q, Tu T, et al. Membrane heat exchanger for novel heat recovery in carbon capture. *J Membr Sci*. 2019;577:60-68.

45. Chen H, Zhou Y, Cao S, et al. Heat exchange and water recovery experiments of flue gas with using nanoporous ceramic membranes. *Appl Therm Eng*. 2017;110:686-694.

46. Mondal S, Field R. Theoretical analysis of the viscosity correction factor for heat transfer in pipe flow. *Chem Eng Sci*. 2018;187:27-32.

47. Li Z, Zhang H, Chen H, Zhang J, Cheng C. Experimental research on the heat transfer and water recovery performance of transport membrane condenser. *Appl Therm Eng*. 2019;160:114060.

48. Yan S, Cui Q, Xu L, Tu T, He Q. Reducing CO_2 regeneration heat requirement through waste heat recovery from hot stripping gas using nanoporous ceramic membrane. *Int J Greenh Gas Control*. 2019;82:269-280.

49. Zhou Y, Chen H, Xie T, Wang B, An L. Effect of mass transfer on heat transfer of microporous ceramic membranes for water recovery. *Int J Heat Mass Transf*. 2017;112:643-648.

50. Kultayeva S, Ha J, Malik R, Kim Y, Kim K. Effects of porosity on electrical and thermal conductivities of porous SiC ceramics. *J Eur Ceram Soc*. 2020;40:996-1004.

51. Huang J, Zhang J, Wang L. Review of vapor condensation heat and mass transfer in the presence of non-condensable gas. *Appl Therm Eng*. 2015;89:469-484.

52. Qin W, Guan K, Lei B, Liu Y, Peng C, Wu J. One-step coating and characterization of $α$-Al_2O_3 microfiltration membrane. *J Membr Sci*. 2015;490:160-168.

53. Cheng C, Zhang H, Chen H. Experimental study on water recovery and SO_2 permeability of ceramic membranes with different pore sizes. *Int J Energy Res*. 2020;44:6313-6324.

54. Zhang W, Ruan X, Ma Y, et al. Modeling and simulation of mitigating membrane fouling under a baffle-filled turbulent flow with permeate boundary. *Sep Purif Technol*. 2017;179:13-24.

55. Tu T, Cui Q, Liang F, Xu L, He Q, Yan S. Water recovery from stripping gas overhead CO_2 desorber through air cooling enhanced by transport membrane condensation. *Sep Purif Technol*. 2019;215:625-633.